

# Optical and X-ray studies of three polars: RX J0859.1+0537, RX J0749.1-0549, and RX J0649.8-0737

Arti Joshi<sup>1\*</sup>, J. C. Pandey<sup>1</sup>, Ashish Raj<sup>2</sup>, K. P. Singh<sup>3</sup>, G. C. Anupama<sup>2</sup>,  
and H. P. Singh<sup>4</sup>

<sup>1</sup>*Aryabhata Research Institute of observational sciencES, Manora Peak, Nainital 263 001, India*

<sup>2</sup>*Indian Institute of Astrophysics, Koramangala, Bangalore 560 034, India*

<sup>3</sup>*Indian Institute of Science Education and Research, Mohali, India*

<sup>4</sup>*Department of Physics and Astrophysics, University of Delhi, 110007 Delhi, India*

Accepted XXX. Received YYY; in original form ZZZ

## ABSTRACT

We present optical photometric and spectroscopic observations, and an analysis of archival X-ray data of three polars: RX J0859.1+0537, RX J0749.1-0549, and RX J0649.8-0737. Optical light curves of these three polars reveal eclipse features that are deep, total, and variable in shape. The optical and X-ray modulations of RX J0859.1+0537, RX J0749.1-0549, and RX J0649.8-0737 are both found to occur at the orbital periods of  $2.393\pm 0.003$  hrs,  $3.672\pm 0.001$  hrs, and  $4.347\pm 0.001$  hrs, respectively. RX J0859.1+0537 is found to be an eclipsing polar which lies in the region of the period gap, whereas RX J0749.1-0549 and RX J0649.8-0737 are found to be long-period eclipsing polars above the period gap. The eclipse length is found to be 61 min for RX J0749.1-0549 in the R-band, which is the highest among the long period eclipsing polars. The radius of the eclipsed light source is found to be more than the actual size of the white dwarf for these three systems, indicating that the eclipsed component is not only the white dwarf but also appears to include the presence of an extended accretion region. Optical spectra of these systems show the presence of high ionization emission lines along with the strong Balmer emission lines with an inverted Balmer decrement. Cyclotron harmonics are also detected in the optical spectra from which we infer magnetic field strength of the surface of the white dwarf to be  $49\pm 2$  MG,  $43.5\pm 1.4$  MG, and  $44\pm 1$  MG for RX J0859.1+0537, RX J0749.1-0549, and RX J0649.8-0737, respectively.

**Key words:** accretion, accretion discs – novae, cataclysmic variables – binaries: eclipsing – stars: individual: RX J0859.1+0537 – stars: individual: RX J0749.1-0549 – stars: individual: RX J0649.8-0737.

## 1 INTRODUCTION

Polars are a class of Magnetic Cataclysmic Variables (MCVs) in which material transfers from Roche lobe-filling red dwarf secondary to a highly magnetized white dwarf. These binary systems are synchronously locked and the formation of an accretion disc is prevented due to a high magnetic field ( $> 10$  MG) on the surface of the white dwarf (WD). The accreted matter follows the magnetic field lines of the WD when the magnetic pressure exceeds the ram pressure (see Cropper 1990; Warner 1995, for a full review of MCVs). The optical and near-infrared radiation

is dominated by the cyclotron emission, while X-ray radiation is dominated by bremsstrahlung emission in hard X-rays. Both bremsstrahlung and cyclotron radiation originate from the magnetically channeled accretion column near the WD in the post-shock region. Cyclotron radiation is highly circularly polarized, reaching 50% in optical bands (see Cropper 1990). The cyclotron cooling is extremely efficient (Lamb & Masters 1979; Woelk & Beuermann 1992), therefore, a part of the downward emitted hard X-rays and cyclotron radiation is absorbed by the WD surface and re-emitted in the soft X-rays or in the extreme UV. The soft X-ray photons are mostly emitted near the base of the post-shock flow and thus a majority of the polars are found to show a ‘soft X-ray excess’.

Observationally, various polars reveal a structured X-

\* E-mail: arti@aries.res.in

ray and photometric eclipse profile. These eclipse profiles are mostly noticed in the high-inclination systems where the white dwarf, the accretion region, and the accretion streams are occulted by the secondary star and provide information about the spatial structures and the binary parameters of the system. Light curves of the eclipse contain information about the structure and the brightness distribution along the stream. The spectroscopic observations of polars can also give further insights into the accretion region. The optical spectra of polars exhibit strong Balmer emission lines along with He I and He II emission lines. The majority of polars have orbital periods shorter than the “period gap (2-3 hrs)”.

The catalogue of [Ritter & Kolb \(2003, update RKcat7.24, 2016, RK\)](#)<sup>1</sup> identified 119 confirmed and 31 uncertain polars. From this catalogue, we took three poorly studied polars namely RX J0859.1+0537 (hereafter RX J0859), RX J0749.1-0549 (hereafter RX J0749), and RX J0649.8-0737 (hereafter RX J0649) for a detailed study. These three systems are identified as polars on the basis of their hardness ratio from *ROSAT* observations ([Beuermann et al. 1995; Motch et al. 1998](#)), and until now there has been no detailed optical and X-ray study carried for these sources, and therefore their exact nature has not been confirmed. The poor knowledge of these sources encouraged us to do the optical (photometric and spectroscopic) and X-ray study. A summary of the available information on these sources is given below.

### 1.1 RX J0859.1+0537

RX J0859 was identified as a polar ([Beuermann et al. 1995; Szkody et al. 2005](#)) using optical spectroscopy and hardness ratio in X-rays. It is located at a distance of  $441\pm 30$  pc ([Gaia Collaboration, Lindegren et al. 2018](#)). From SDSS spectra obtained during 2003, [Szkody et al. \(2005\)](#) found the orbital period of 1.1 hrs but later [Gänsicke & Dillon \(2009\)](#) re-analysed the SDSS spectrum and derived the orbital period of  $\sim 2.4$  hrs. [Harrison & Campbell \(2015\)](#) found that the WISE (Wide-field Infrared Survey Explorer) W1 ( $=3.4 \mu\text{m}$  wavelength band) light curve of RX J0859 folded reasonably well with a period of 1.1 hrs, while the source was not found to vary in WISE W2 ( $=4.6 \mu\text{m}$  wavelength band) light curve. [Harrison & Campbell \(2015\)](#) have also estimated the field strength of RX J0859 between 20 -35 MG after attributing the humps in the W1 light curve to cyclotron emission.

### 1.2 RX J0749.1-0549

RX J0749 was first identified by [Motch et al. \(1998\)](#) among the *ROSAT* Galactic Plane Survey sources located at low galactic latitudes. They reported it to be a long period polar with an orbital period of  $\sim 3.6$  hrs. Using Gaia DR2 parallax the distance of RX J0749 is calculated to be  $1168\pm 164$  pc ([Gaia Collaboration, Lindegren et al. 2018](#)).

### 1.3 RX J0649.8-0737

[Motch et al. \(1998\)](#) characterized RX J0649 as a polar with an orbital period of  $\sim 4.4$  hrs. It is located at a distance

**Table 1.** A log of photometric, spectroscopic, and X-ray observations of RX J0859.1+0537, RX J0749.1-0549, and RX J0649.8-0737.

Object	Date of Obs.	Telescope	Instrument	Filter/ band	Integration Time (s)	Time (HJD <sub>r</sub> )	Time span(hr)
RX J0859	2014 Jan 30	1.3-m	CCD	R	250	2456688.00	2.5
	2014 Jan 31	1.3-m	CCD	R	200	2456689.00	2.6
	2014 Feb 23	1.3-m	CCD	R	250	2456712.00	3.4
	2014 May 03	1.04-m	CCD	R	300	2456781.00	1.8
	2015 Mar 27	1.04-m	CCD	R	300	2457105.00	3.7
	2015 Apr 09	1.04-m	CCD	R	300	2457122.00	3.3
	2015 Apr 10	1.04-m	CCD	R	300	2457123.00	2.8
	2017 Dec 22	2.01-m	HFOSC/Gr07	380-780 nm	3600	2458110.43	1.0
	1996 Apr 24	ROSAT	HRI	0.1-2.2 keV	32846	2450197.95	433.2
	RX J0749	2014 Jan 30	1.3-m	CCD	R	250	2456688.00
2014 Jan 31		1.3-m	CCD	R	250	2456689.00	2.8
2014 Apr 24		1.3-m	CCD	R	250	2456772.00	2.5
2014 Apr 25		1.3-m	CCD	R	250	2456772.00	2.4
2015 Jan 23		1.04-m	CCD	R	300	2457046.00	4.9
2015 Jan 16		1.04-m	CCD	R	300	2457129.00	1.8
2017 Dec 22		2.01-m	HFOSC/Gr07	380-780 nm	3600	2458110.34	1.0
1997 Apr 09		ROSAT	HRI	0.1-2.2 keV	45490	2450548.02	203.1
RX J0649	2015 Nov 06	1.3-m	CCD	R	200	2457333.00	3.7
	2015 Nov 21	1.3-m	CCD	R	200	2457348.00	4.5
	2015 Dec 19	1.3-m	CCD	R	250	2457376.00	3.3
	2017 Dec 22	2.01-m	HFOSC/Gr07	380-780 nm	3600	2458110.19	1.0
	1997 Sept 23	ROSAT	HRI	0.1-2.2 keV	17080	2450714.97	4.7

*Note.*- HJD<sub>r</sub> for HFOSC and HRI instrument is the start time of the observations, whereas for optical observation it is observation day.

**Table 2.** Comparison stars used for the differential photometry for RX J0859.1+0537, RX J0749.1-0549, and RX J0649.8-0737.

Object	Reference USNO-B1.0	B (mag)	R (mag)
RX J0859	0956-0174607	19.42	16.93
‘C1’	0956-0174599	17.55	16.34
‘C2’	0956-0174609	16.83	16.13
RX J0749	0841-0159780	17.36	17.75
‘C1’	0841-0159756	17.30	16.96
‘C2’	0841-0159759	16.46	16.17
RX J0649	0823-0138560	18.80	16.69
‘C1’	0823-0138520	17.58	16.31
‘C2’	0823-0138559	17.02	16.51

*Note.*- Here, C1 and C2 stands for comparison 1 and 2 for each program star.

of  $611\pm 38$  pc ([Gaia Collaboration, Lindegren et al. 2018](#)). WISE W1 light curves of RX J0649 show an ellipsoidal variation with a period of 4.4 hrs (see [Harrison & Campbell 2015](#)). However, the WISE W2 light curve, seems to be deeper, and has a shorter-lived minimum than in W1. [Harrison & Campbell \(2015\)](#) also suggested that the WISE W2 light curve was more consistent with a strong cyclotron emission with magnetic field  $B \leq 26$  MG. From near-IR colors they reported that the secondary star is consistent with an early M-type star.

This paper is organized as follows: we summarize our optical observations and data reduction in the next section. Section 3 contains analyses and the results of the optical and X-ray data. Finally, we present discussion and conclusions in sections 4 and 5, respectively.

<sup>1</sup> <https://wwwmpa.mpa-garching.mpg.de/RKcat/cbcat>

**Table 3.** The times of eclipse minima of RX J0859.1+0537, RX J0749.1-0549, and RX J0649.8-0737.

Object	Date of Obs.	Eclipse Minima (HJD <sub>t</sub> +)	Cycles
RX J0859	2014 Jan 30	0.426723±0.044333	0
	2014 Jan 31	0.426093±0.041722	10.00
	2014 Feb 23	0.318837±0.028185	239.00
	2015 Mar 27	0.131961±0.022238	4169.97
	2015 Mar 27	0.231166±0.042367	4170.96
	2015 Apr 09	0.124104±0.019132	4340.01
RX J0749	2015 Apr 10	0.221810±0.047712	4350.99
	2014 Jan 31	0.285211±0.002894	0
	2014 Apr 24	0.107516±0.002894	537.02
RX J0649	2015 Jan 23	0.308878±0.003472	2314.95
	2015 Apr 16	0.126693±0.003472	2851.95
	2015 Nov 06	0.451228±0.067288	0
	2015 Nov 21	0.479756±0.051732	81.97
	2015 Dec 19	0.329473±0.079010	233.88

Note.- HJD<sub>t</sub> is similar to the values defined in the Table 1.

## 2 OBSERVATIONS AND DATA REDUCTION

### 2.1 Optical Photometry

R-band photometric observations of these sources were obtained in 2014 and 2015 using the 1.04-m Sampuranand Telescope (ST) at ARIES, Nainital (Sinval et al. 1975) and 1.3-m Devasthal Fast Optical Telescope (DFOT) located at Devasthal, Nainital, India (Sagar et al. 2011). A detailed log for photometric observations is given in Table 1. The ST has Ritchey-Chretien (RC) optics with a f/13 beam at the Cassegrain focus. The ST is equipped with a 2k×2k Andor CCD (read noise=13.7  $e^- pixel^{-1}$  and gain=10  $e^-/Analog$  to Digital Unit (ADU)). CCD covers a field-of-view (fov) of 13'×13' and its each pixel has a dimension of 24  $\mu m^2$ . Observations were carried out in a 2×2 pixel<sup>2</sup> binning mode in order to increase the signal-to-noise ratio. The 1.3-m DFOT is also RC design with f/4 beam at the Cassegrain focus. The DFOT is equipped with a 2k×2k Andor CCD (read noise=7  $e^- pixel^{-1}$  and gain=2  $e^-/ADU$  at 1 MHz readout speed). Each pixel size of the CCD is 13.5  $\mu m^2$  and covers a total field of ~18'×18'. Photometric observations of RX J0649 were also carried out from DFOT with a 512 × 512 Andor CCD (read noise = 6.1  $e^- pixel^{-1}$  and gain=10  $e^-/ADU$  at 1 MHz readout speed) with a pixel size of 13.5  $\mu m^2$  and the fov of the CCD is 5 arcmin on the sky. Several bias and twilight sky flat frames were taken during the observing runs. The pre-processing (bias subtraction, flat fielding, and cosmic ray removal) of the raw photometric data were performed using IRAF<sup>2</sup> software. Differential photometry (variable minus comparison star) was performed by using a comparison star in the same field. The details of the adopted comparison stars for each source are given in Table 2. The instrumental magnitudes of the target and two comparison stars labelled as 'C1' and 'C2' were extracted from the images. Then the R-band magnitudes of observations were computed with re-

spect to comparison star 'C1'. The nightly variations ( $\sigma$ ) of 'C1-C2' were found to be in the range of 0.005-0.01 (for RX J0859), 0.007-0.01 (for RX J0749), and 0.009-0.01 (for RX J0649), respectively. The standard magnitude of 'C1' and 'C2' were taken from USNO-B1.0 catalogue (see Table 2). The constant brightness of comparison stars was checked by inspecting the light curves of 'C1-C2' for each source separately.

### 2.2 Optical Spectroscopy

Long-slit low-resolution optical spectra for these polars were obtained on 22 December 2017 with the 2.01-m Himalayan Chandra Telescope at IAO, Hanle which is equipped with the Hanle Faint Object Spectrograph and Camera (HFOSC). We used the Gr7 (3800-7800 Å) grism with resolution of 1330 for our observations. Exposure time was 3600 s for each observation in order to obtain good S/N spectra. Spectrophotometric standards were also observed during our observations. Detailed information about the spectroscopic observations is provided in Table 1. The spectra of target and standard stars were extracted in the standard manner using IRAF tasks. In the extracted one dimensional spectrum the abscissa corresponds to the pixel number and ordinate is in the form of intensity. Lamp spectra of FeAr have been used for the wavelength calibration. The wavelength calibration was accomplished by using the IRAF-task IDENTIFY, which determines the pixel-to-wavelength solution for arc spectrum. To execute this solution to the extracted spectrum of the standard star and target, the task DISPCOR is used. To check the wavelength calibration, the night sky emission lines 5577 Å, 6300 Å, and 6363 Å were used and an appropriate shift is applied where necessary. The flux calibration was performed by using the tasks STANDARD, SENSFUNC, and CALIBRATE in IRAF. Therefore, the flux calibrated one-dimensional spectra finally provide the distribution of flux over wavelength. The telluric lines were not removed from the spectra.

### 2.3 X-ray Data

The archival X-ray data were obtained from the ROSAT observations of RX J0859, RX J0749, and RX J0649 that were carried out on 24 April 1996, 09 April 1997, and 23 September 1997, respectively using the High-Resolution Imager (HRI; Zombeck et al. 1995). A log of observations is given in Table 1. ROSAT has ~ 40' diameter fov with the HRI in the focal plane observing in the energy range of ~ 0.1-2.2 keV. HRI consisted of two cascaded microchannel plates (MCPs) with a crossed grid position readout system and provided a 38'×38' field-of-view with ~ 2'' spatial resolution (FWHM). HRI used a crossed grid detector with a position accuracy to 25 micrometers. This instrument had also a very low or negligible energy resolution but provided time resolution down to 61  $\mu s$  relative to the ROSAT spacecraft clock. The X-ray image and the light curves of these sources were extracted by using the XSELECT task in the FTOOLS package. The X-ray light curves of each source were obtained using a circular region with a radius of 25'' centered on the source. The background regions were taken from a source-free region around the source in the same data. Finally, the

<sup>2</sup> IRAF is distributed by the national optical astronomy observatories, USA.

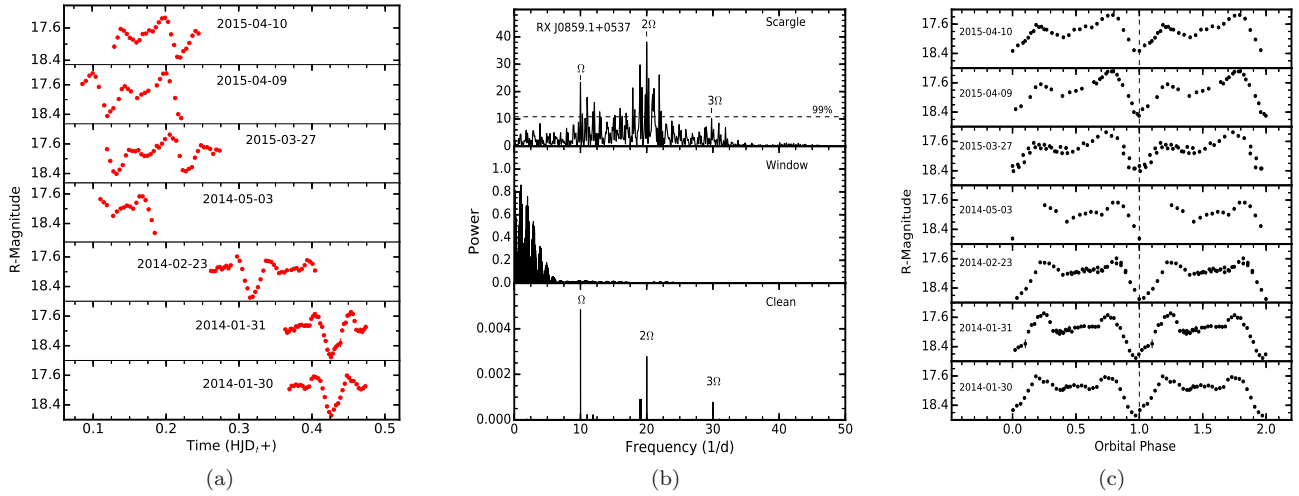


**Figure 1.** (a) R-band light curve of RX J0859.1+0537, (b) Lomb-Scargle power spectra (top panel), window function (middle panel), and CLEANed power spectra (bottom panel) of RX J0859.1+0537, and (c) folded R-band light curve of RX J0859.1+0537. The date of observations are mentioned near each light curve. The  $HJD_t$  of each observation is given in Table 1.

**Table 4.** Periods corresponding to dominant peaks in the power spectra of RX J0859.1+0537, RX J0749.1-0549, and RX J0649.8-0737 obtained from X-ray and optical data.

Object	Period (hr)	SCARGLE		CLEAN	
		Photometry	ROSAT	Photometry	ROSAT
RX J0859	$P_\Omega$	2.40±0.02	2.43±0.04	2.398±0.020	2.393±0.003
	$2P_\Omega$	1.20±0.01	1.23±0.02	1.203±0.001	1.261±0.001
	$3P_\Omega$	0.80±0.01	0.80±0.01	0.799±0.003	0.812±0.003
RX J0749	$P_\Omega$	3.75±0.11	3.68±0.02	3.672±0.001	3.675±0.002
RX J0649	$P_\Omega$	4.32±0.20	4.34±0.13	4.310±0.002	4.347±0.001
	$3P_\Omega$	1.42±0.14	1.26±0.10	1.482±0.001	1.251±0.001

background subtracted X-ray light curves were obtained by using the task LCMATH. The temporal binning for each light curve was 16 s.

### 3 ANALYSIS AND RESULTS

#### 3.1 RX J0859.1+0537

##### 3.1.1 Optical Photometry

We obtained a total of 20.1 hrs of photometric data from our observations carried out over seven nights. R-band photometric light curves of RX J0859 are shown in Figure 1(a). Light curves of each epoch of observations exhibit a clear eclipse profile where the brightness of the system dropped by an average of  $\sim 1.1$  mag. To know the orbital period and the eclipse morphology of RX J0859, we determined mid-eclipse times (see Table 3) by fitting parabolas to the bottom part of eclipses for all epochs of observations except one - the epoch of 03 May 2014 (where the whole eclipse profile was not observed). A linear least square fit to the seven eclipse timings provides the following ephemeris for RX J0859:

$$T_0 = HJD2456688.4296(19) \pm 0.0999294(6)E, \quad (1)$$

where  $T_0$  is defined as the time of mid-eclipse and the errors are given in brackets.

The orbital period of RX J0859 was thus derived to be 2.39 hrs. A careful visual inspection showed that the primary eclipse going to complete one cycle during 27 March 2015 and 09 April 2015 provided an estimate of the orbital period of  $\sim 2.4$  hrs. We have also performed the period analysis of RX J0859 by applying Fourier Transform (FT) to the photometric data and using the Lomb-Scargle periodogram algorithm (see Lomb 1976; Scargle 1982; Horne & Baliunas 1986). The Lomb-Scargle power spectrum of RX J0859 is shown in the top panel of Figure 1(b). Various peaks are observed in the power spectrum as the fundamental and harmonics of the orbital period. These peaks are marked as  $\Omega$ ,  $2\Omega$ , and  $3\Omega$ . The errors on these periods are derived by using the method given in (Horne & Baliunas 1986). The significance of this detected peaks is determined by calculating the false alarm probability (see Horne & Baliunas 1986). The horizontal line shows a 99% significance level. The Scargle power spectrum of RX J0859 is noisier due to data gaps. Therefore, true variations in the source are further modulated by the irregular sampling defined by the window function of the data. We have computed the window function with the same time sampling but contains only a constant magnitude and is shown in the middle panel of Figure 1(b). The frequencies identified in the Lomb-Scargle power spectrum did not fall under the window function, which assures that the periods derived from the Lomb-Scargle power spectrum are real. In order to further confirm the periodicity of this system, the CLEAN algorithm (Roberts et al. 1987) is applied to the data. Lower panel of Figure 1(b) shows the CLEANed power spectrum of all photometric data of RX J0859. The CLEANed power spectrum was obtained with a loop gain of 0.1 and 1000 iteration. Similar to the Scargle periodogram, the peaks corresponding to the frequencies  $\Omega$ ,  $2\Omega$ , and  $3\Omega$  are also found in the CLEANed power spectrum. The error in the period obtained from CLEAN method is determined as  $P^2/2t_{max}$ , where  $P$  is the period and  $t_{max}$  is the duration of the observations (see Roberts et al. 1987). The periods corresponding to these frequencies are given in



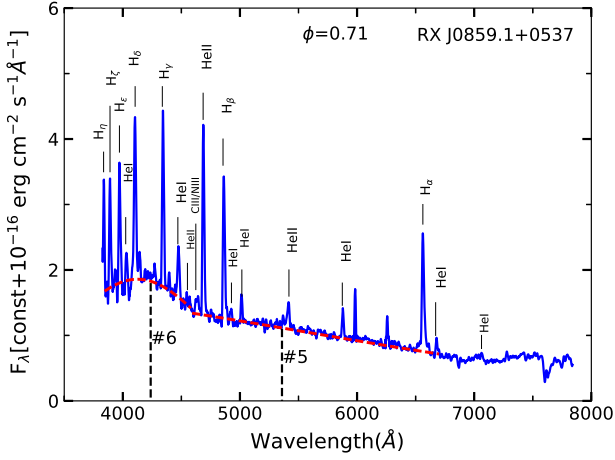


**Figure 2.** Optical spectrum of RX J0859.1+0537. The orbital phase of the observation is mentioned at the top of the spectrum. The overlaid solid dash red lines are the best fitted Gaussian to the cyclotron hump after excluding the emission lines. Vertical dashed lines represent the cyclotron humps and corresponding cyclotron harmonic numbers are also mentioned.

Table 4. These power spectral analysis further confirms that the derived orbital period of RX J0859 is  $2.393 \pm 0.003$  hrs.

The photometric light curves of all these seven observations were also folded using the ephemeris given in equation 1 and are shown in Figure 1(c). Most of the light curves show a V-shape eclipse profile, whereas the light curve of 27 March 2015 exhibits a relatively flat bottom of the eclipse.

The mass ( $M_2$ ) and radius ( $R_2$ ) of the secondary are estimated to be  $0.19 \pm 0.07 M_\odot$  and  $0.24 \pm 0.03 R_\odot$ , respectively with the help of the mean empirical mass-period relation of Smith & Dhillon (1998). We have estimated the mean density ( $\bar{\rho}$ ) of secondary as  $18.6 \pm 0.1 \text{ g cm}^{-3}$  (see Warner 1995, for formulae). This mean density of secondary corresponds to a lower main sequence star of spectral class M4 and an effective temperature of 3300 K (see Beuermann et al. 1998; Knigge 2006). Using the mass range of WD of 0.2-1.5  $M_\odot$  in CVs (Zorotovic et al. 2011), the binary separation (a) is estimated to be in the range of  $(4.6 - 7.5) \times 10^{10}$  cm.

### 3.1.2 Optical Spectroscopy

A very rich optical spectrum with a wealth of spectral features was obtained at out-of-eclipse phase  $\phi=0.71$  for RX J0859 and is shown in Figure 2. Identification, fluxes, equivalent width (EW), and FWHM of the principal emission lines of RX J0859 obtained through a single-Gaussian fitting are given in Table 5. The optical spectrum is dominated by the single-peaked Balmer emission lines (from H $\alpha$  to H $\eta$ ). The high-excitation line He II 4686 Å is quite prominent and its strength is 6/5 of the H $\beta$ -flux. Several emission lines of He I, He II, and the Bowen fluorescence lines are also present in the optical spectrum of RX J0859. The Bowen fluorescence line is observed with the NIII line along with an additional contribution from CIII. In addition to He II 4686 Å line, we have also found a weak He II 4542 Å emission line from

the Pickering series. Schachter et al. (1991) reported that the Pickering series is also observed in few AM Her systems. The flux ratio of He II 4542 Å to He II 4686 Å is found to be 0.1.

Two broad features are clearly observed in the optical spectrum of RX J0859 and are identified as due to cyclotron emission that occurs at discrete harmonics of cyclotron frequency. Unlike the first hump, the second hump appears to be shallower in this system. These humps are equally spaced in frequency for a given electron at low energies where the relativistic effects are not important. The central wavelength of each cyclotron hump was estimated by fitting the Gaussian curve. The error corresponds to the central wavelength of each hump is the standard deviation obtained from the Gaussian fitting. Any measurement of the position of the cyclotron hump is problematic by the intense emission lines in the spectrum. Thus, the emission lines were removed while fitting the Gaussian to the hump. The dashed line overlaid in the spectrum in Figure 2 shows the best fit Gaussian curve to the cyclotron humps. We have identified prominent humps at  $4238 \pm 191$  Å and  $5359 \pm 407$  Å. If we consider these two humps as successive harmonics of fundamental cyclotron frequency ( $\nu_{cyc}$ ), their separation provides the measured humps at 4238 Å and 5359 Å as the 6<sup>th</sup> and 5<sup>th</sup> harmonics of fundamental cyclotron frequency, respectively. For a given magnetic field, the fundamental cyclotron frequency is described as  $\nu_{cyc} = 2.8 \times 10^{12} B_6$  Hz or  $\omega_B = 2 \pi \nu_{cyc} = 1.76 \times 10^{13} B_6$  (see Ingham et al. 1976; Warner 1995). However, the exact value of the magnetic field will, in fact be, depend on the temperature of the plasma and the viewing angle relative to the field lines (for more detail see Wickramasinghe & Meggitt 1982; Barrett & Channugam 1985). Here,  $B_6$  is magnetic field in terms of  $10^6$  G. Using the value of  $\omega_B$ , the equation (3) of Cropper (1989) can be written as

$$B_6 = \frac{4.28 \times 10^6 \sin^2 \theta}{\mu \lambda \left[ -1 + \sqrt{1 + (8n \sin^2 \theta / \mu)} \right]} \quad (2)$$

where  $\lambda$  is in the unit of Å,  $\mu = m_e c^2 / kT = 511.1 / T$ ,  $T$  is the plasma temperature in the unit of keV,  $n$  is the cyclotron harmonic number, and  $\theta$  is the viewing angle to the magnetic field line. In order to determine the magnetic field strength, we have tried to constrain the temperature  $T$  and the viewing angle  $\theta$  for which the consistent magnetic field for both observed harmonics can be determined. For  $T=10$  keV and  $\theta=90^\circ$ , we have estimated the consistent magnetic field of  $50 \pm 2$  MG and  $B=47 \pm 4$  MG for the 6<sup>th</sup> and 5<sup>th</sup> harmonics, respectively. These values of the estimated magnetic field were well within the  $1\sigma$  level. The uncertainty on  $B$  was derived from uncertainty in the central wavelength of cyclotron harmonics. Thus, the average value of the magnetic field strength of the WD in the system RX J0859 is estimated to be  $49 \pm 2$  MG.

### 3.1.3 X-ray Timing Analysis

The background subtracted ROSAT-HRI light curve was extracted for one long exposure of RX J0859. Data gaps were seen in the light curve of RX J0859 due to the occultation of the source by the Earth. Periodicity in the X-ray data

**Table 5.** Identification, flux, EW, and FWHM for emission features of RX J0859.1+0537, RX J0749.1-0549, and RX J0649.8-0737.

Identification	RX J0859.1+0537			RX J0749.1-0549			RX J0649.8-0737		
	Flux	-EW	FWHM	Flux	-EW	FWHM	Flux	-EW	FWHM
H $\eta$ (3835 Å)	1.36	7	1839	1.26	7	1026	3.25	7	1281
H $\zeta$ (3889 Å)	2.83	17	1990	1.50	10	1152	4.79	11	1255
H $\zeta$ (3970 Å)	3.15	18	1357	2.65	20	1194	6.62	15	1369
HeI (4026 Å)	1.22	7	1482	0.47	3	1640	1.11	3	1104
H $\delta$ (4102 Å)	4.87	25	1678	9.39	53	949	8.15	16	1392
H $\gamma$ (4340 Å)	4.75	27	1417	3.51	19	1322	9.86	20	1319
HeI (4471 Å)	2.01	13	1802	1.28	8	2122	3.09	7	1529
HeII (4542 Å)	0.30	2	925	0.31	2	1752	1.42	5	2591
CIII/NIII (4640/50 Å)	0.49	4	1872	0.41	1	1229	1.05	4	2500
HeII (4686 Å)	4.96	36	1296	1.37	9	1853	5.93	14	1122
H $\beta$ (4861 Å)	4.21	34	1348	3.01	22	1318	9.76	24	1287
HeI (4922 Å)	0.42	4	1304	0.31	2	1407	1.27	3	1045
HeI (5016 Å)	0.62	5	1060	..	..	..	1.03	3	837
FeII (5169 Å)	..	..	..	0.40	3	1854	1.06	3	1568
HeII (5412 Å)	0.60	5	1179	..	..	..	1.80	4	1718
HeI (5875 Å)	0.77	8	1044	1.19	9	1619	2.28	6	920
H $\alpha$ (6563 Å)	3.57	42	1093	2.32	19	886	9.20	27	971
HeI (6678 Å)	0.58	8	1168	1.01	5	1149	1.42	5	988
HeI (7065 Å)	0.64	10	3151	0.40	5	1481	1.26	5	1676

Note.- Flux, EW, and FWHM are in the unit of  $10^{-15}$  erg cm $^{-2}$  s $^{-1}$ , Å, and km s $^{-1}$ , respectively.

of RX J0859 was searched by using similar methods as discussed above. The X-ray power spectra of RX J0859 using Lomb-Scargle and CLEAN algorithms along with the window function are shown in Figure 3. The highest peaks in both Lomb-Scargle and CLEAN power spectra correspond to the orbital period of 2.4 hrs and its harmonics at 1.2 hrs and 0.8 hrs. These values of the period are found to be consistent with those derived from the optical light curves. Also, no window pattern is seen near these frequencies (see also middle panel Figure 3). The X-ray light curve of RX J0859 was also folded with the ephemeris as given in equation 1. The orbital modulation is clearly observed and confirms the orbital period of RX J0859. A double-humped structure is seen in the phased X-ray light curve. The prominent hump is near the orbital phase  $\sim 0.5$ , while the secondary hump is observed at phase  $\sim 0.85$  with a smaller amplitude.

### 3.2 RX J0749.1-0549

#### 3.2.1 Optical Photometry

RX J0749 was observed for a total of  $\sim 17$  hrs in six nights. Figure 5(a) shows the R-band photometric light curves of RX J0749. Ellipsoidal variations are clearly visible in each epoch of observations. The profiles of eclipses are complicated and highly variable. We used the mid-eclipse times for all observations, except for 25 April 2014 and 30 January 2014, for the best determination of ephemeris. The entire eclipse profile was not covered in the two observations excluded here. We also take half the exposure time as the uncertainty in the measurement of mid-eclipse for all four observations. This approach is similar to that mentioned in section 3.1.1, and the ephemeris thus determined for the time of mid-eclipse is given as

$$T_0 = HJD2456688.28521(3) \pm 0.154225(2)E. \quad (3)$$

We thus find that the orbital period of RX J0749 is 3.7014 hrs. A full eclipse was seen during the epoch 23 January 2015 due to the sufficient data length as compared to other epochs of observations. A clear flat bottom was also

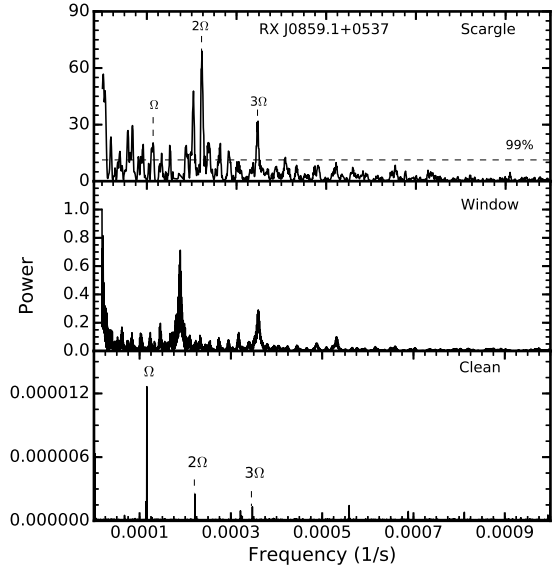


**Figure 3.** Lomb-Scargle X-ray power spectra (*top panel*), window function (*middle panel*), and CLEANed X-ray power spectra (*bottom panel*) of RX J0859.1+0537. The horizontal dash line represent 99% significance level.

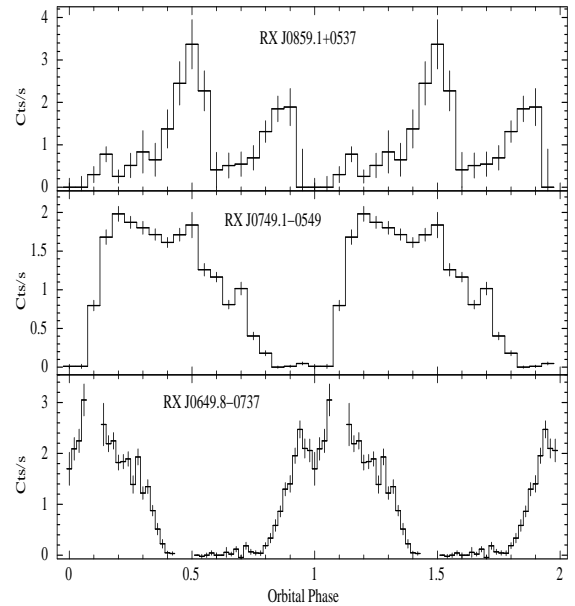


**Figure 4.** Orbital phase folded X-ray light curves of RX J0859.1+0537, RX J0749.1-0549, and RX J0649.8-0737 in energy range 0.1-2.2 keV.

observed in this observation, where the time duration of total eclipse was  $\sim 61$  min. Power spectra of RX J0749 are shown in the Figure 5(b). The period corresponding to the peak frequency is given in Table 4. The CLEAN algorithm leads to an orbital period of  $3.672 \pm 0.001$  hrs, however. As shown in middle panel of Figure 5(b), no window pattern is seen near the identified orbital frequency. The light curves of all six observations were also folded using the ephemeris given in equation 3 and are shown in Figure 5(c). Each light curve of RX J0749 shows a noticeable change in the shape of the eclipse profile. The brightness of RX J0749 was found

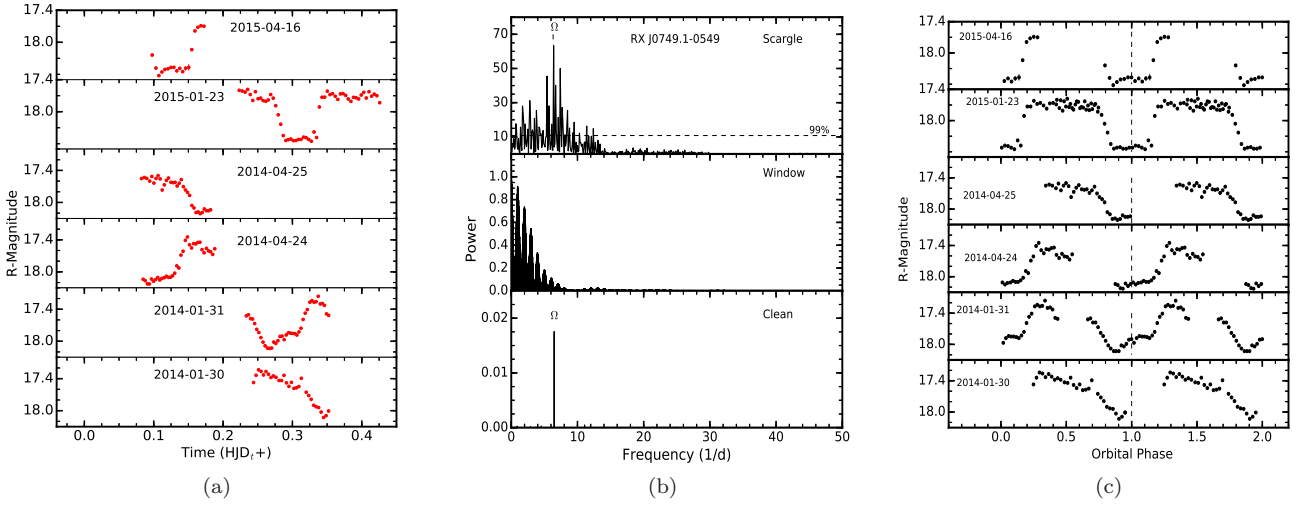


**Figure 5.** (a) R-band light curve of RX J0749.1-0549, (b) Lomb-Scargle power spectra (top panel), window function (middle panel), and CLEANed power spectra (bottom panel) of RX J0749.1-0549, and (c) folded R-band light curve of RX J0749.1-0549. The date of observations are mentioned near each light curve. The  $HJD_t$  of each observation is given in Table 1.

to be decreased from the year 2014 to the year 2015 by  $\sim 0.4$  mag. The eclipse profile was also observed to be more symmetric and flat-bottomed in the year 2015.

The mass and radius of the secondary have been derived to be  $0.35 \pm 0.08 M_{\odot}$  and  $0.39 \pm 0.03 R_{\odot}$ , respectively, using the same procedure as above. We have also estimated the separation between the WD and secondary in the range of  $(6.88 - 10.3) \times 10^{10}$  cm assuming  $M_1 = (0.2 - 1.5) M_{\odot}$ . Using the orbital period of  $3.672 \pm 0.001$  hrs, the mean density of secondary is calculated to be  $\bar{\rho} = 7.940 \pm 0.004 \text{ g cm}^{-3}$  which indicates that the secondary of RX J0749 has a spectral type of M3.7 and an effective temperature of 3400 K.

### 3.2.2 Optical spectroscopy

Low-resolution spectrum of RX J0749 was obtained at an orbital phase of 0.74 and is shown in Figure 6. The spectrum is dominated by the Balmer emission lines, He II 4686 Å emission features along with the lines of He I, He II, and the Bowen CIII/NIII. In contrast to RX J0859, the strength of the He II 4686 Å emission line is relatively weak and corresponds to 7/5 of the  $H\beta$ -flux. The emission line of Fe II 5169 Å is also visible in the spectrum of RX J0749. The flux ratio of He II 4542 Å to He II 4686 Å is found to be  $\sim 0.2$ . The parameters derived from the optical spectrum of RX J0749 are given in Table 5.

As in the case of RX J0859, two cyclotron humps with variable amplitude are also seen in the optical spectrum of RX J0749. Following the method described above, the central wavelengths of these humps were found to be  $4344 \pm 171$  Å and  $5382 \pm 279$  Å and are identified as  $6^{th}$  and  $5^{th}$  harmonics of a fundamental cyclotron frequency, respectively. Considering  $T$  of 9 keV and  $\theta$  of  $40^\circ$ , comparable magnetic field strengths of  $44 \pm 2$  MG for  $6^{th}$  harmonic and  $43 \pm 2$  MG for  $5^{th}$  harmonic were found. This reveals an average field strength of  $43.5 \pm 1.4$  MG for RX J0749.

### 3.2.3 X-ray Timing Analysis

The power spectra of the X-ray light curve of RX J0749 as obtained from Lomb-Scargle and CLEAN periodograms are shown in the top and bottom panels of Figure 7. The highest peak in both Lomb-Scargle and CLEANed power spectra corresponds to the orbital period of  $\sim 3.68$  hrs, which is similar to that derived from the R-band light curve (see Table 4). As shown in the middle panel of Figure 7, no windowing is seen near the significant peak in the Lomb-Scargle power spectrum. The X-ray light curve was folded with the derived ephemeris as given in equation 3. The folded light curve is shown in the middle panel of the Figure 4. The orbital modulation appears to be maximum around phases  $\sim 0.25$  and interrupted by a broad, eclipse-like feature centered around the orbital phase 1.0, as seen in the R-band light curve.

## 3.3 RX J0649.8-0737

### 3.3.1 Optical Photometry

The R-band light curves of RX J0649 are shown in Figure 8(a) for three sets of observations. A total of 11.5 hrs of data were obtained for this object. The ephemeris for the time of mid-eclipse (see Table 3) deduced from the three observations is

$$T_0 = HJD2457333.451484(20) \pm 0.183337(4)E. \quad (4)$$

Lomb-Scargle, window function, and CLEANed power spectra of the R-band light curves of this system are shown in Figure 8(b). A period of  $4.310 \pm 0.002$  hrs is found corresponding to the highest peak in the CLEANed power spectrum, which is close to that seen in the Lomb-Scargle power spectrum. This peak is also found to be free from any spectral window. We interpret this period as the orbital period of the system. The significant second harmonic of the orbital period is also detected in both power spectra. The light curves for all epochs of observations were folded using the period of 4.34 hrs and are shown in Figure 8(c). For each observation, the optical variations show a well-defined and deep eclipse-







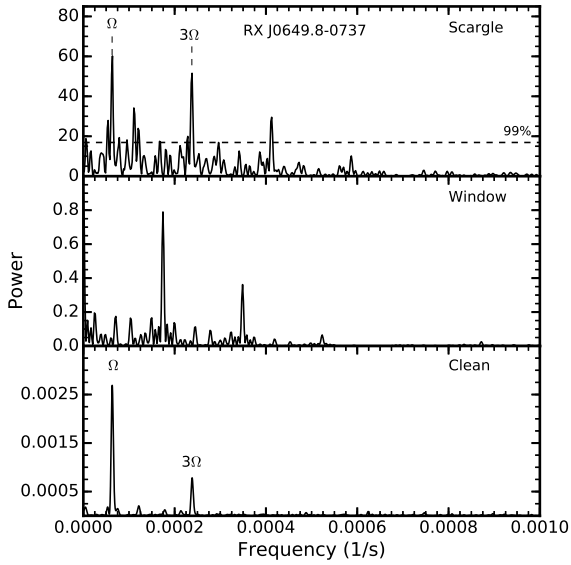


**Figure 10.** Lomb-Scargle X-ray power spectra (*top panel*), window function (*middle panel*), and CLEANed X-ray power spectra (*bottom panel*) of RX J0649.8-0737. The horizontal dash line represent 99% significance level.

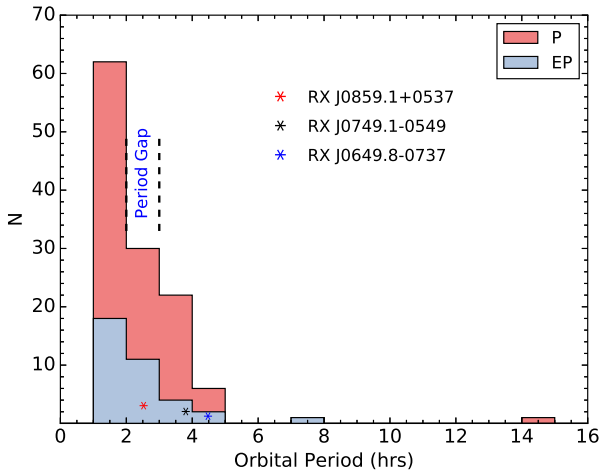


**Figure 11.** The period distribution for confirmed polars (P) and eclipsing polars (EP) taken from RK catalogue. The population of eclipsing polars also includes the newly identified eclipsing polars in this study and are represented by symbol stars.

ure 12. Here,  $R$  is derived in terms of the radius of WD ( $R_{WD}$ ), where  $R_{WD}$  is estimated using the mass-radius relation given by Nauenberg (1972). The limiting values of  $q$  are estimated by using the minimum and maximum values of WD in CVs of  $0.2 M_{\odot}$  and  $1.5 M_{\odot}$ , respectively (see Zorotovic et al. 2011). For the average value of  $q$  of 0.24 (assuming the average value of the mass of WD in CVs as  $0.8 M_{\odot}$ ; Zorotovic et al. 2011), the value of  $R$  is estimated to be  $\sim 40 R_{WD}$ . Even for the maximum value of the  $q$ , the value of  $R$  is estimated to be more than  $18 R_{WD}$  for RX J0859. The large value of  $R$  indicates that the eclipse observed in the light curves is not solely due to the occultation

of WD by secondary. In general, the dimension of the optical and X-ray emission sites are thought to be  $< 0.1 R_{WD}$  (Bailey & Cropper 1991). Therefore, the observed eclipse in RX J0859 might be due to the occultation of the accretion spot on the WD and an extended stream or an extended magnetic accretion region on the WD surface. Such large eclipsing regions were also observed in other well known eclipsing polars like V895 Cen (Stobie et al. 1996), V1432 Aql (Watson et al. 1995), and HU Aqr (Hakala et al. 1993).

The presence of double hump bright phase in the R-band light curve of RX J0859 suggests that both accreting poles are always visible and cyclotron radiation is present along the line of sight of the observer. The low flux observed during the phase  $\sim 0.3-0.6$  with respect to bright phases indicates that cyclotron emitting region might be behind the white dwarf during this time. The amplitudes of double hump bright phase are found to be changing from one observation to another indicating a variable accretion rate. The X-ray orbital modulations of RX J0859 also reveals two humps in an orbital cycle with different amplitude. The first hump was found to have a larger amplitude than the second hump. Double hump like structures have also been reported in the X-ray light curves of other polars MT Dra (Schwarz et al. 2002), WX LMi (Vogel et al. 2007), DP Leo (Pandel et al. 2002), and WW Hor (Pandel et al. 2002) etc., where the activity from the second pole is lower as compared to the primary in few polars, while few of them are equally accretes from both poles. Therefore, in the case of RX J0859, the unequal double hump in the light curve indicates that both poles of the WD emit the radiation unequally due to the different magnetic field strength and mass accretion rate.

R-band photometric light curves of RX J0749 show that the morphology of the eclipse profile changes from one epoch of observations to other. In the observation on 23 January 2015, the flat bottom eclipse profile was observed for RXJ0749 and where the width of the eclipse was observed to be  $\sim 61$  min. This duration is too long among polars to represent an eclipse of just the primary star. The value of  $\Delta\phi_{ie}$  for RX J0749 is derived to be  $0.16 \pm 0.01$ . For an average value of  $q$  of 0.44 and  $i \sim 80^\circ$ , the value of  $R$  is estimated to be  $\sim 50 R_{WD}$  for RX J0749. As shown in Figure 12, for the extreme low and high values of  $q$ ,  $R$  is estimated to be  $\sim 88 R_{WD}$  and  $\sim 23 R_{WD}$ , respectively for RX J0749. Thus the estimated radius of eclipsed light source represents the eclipse feature might be observed due to the obscuration of both an extended stream and hot compact accretion region. The fluctuations in the eclipse parameters like eclipse profiles, eclipse width, the duration of ingress and egress, and the dipper phasing are also observed in the light curves from all the observations. The brightness of RX J0749 is also decreased from the epoch 2014 to the epoch 2015, indicating that this system has undergone a transition from a high state in 2014 to a low state in 2015. These changes can tentatively be explained by the variation in the accretion rate, the size, density, and location of the accretion region. However, small changes in the stream trajectory will also produce changes in the absolute phasing of the dips. The photometric variations as seen on 23 January 2015 are also found to be similar to that of few other eclipsing polars like UZ For, MN Hya, V1309 Ori, and V1432 Aql etc. (see Bailey & Cropper 1991; Buckley et al. 1998; Staude et al. 2001; Watson et al. 1995). Soft X-ray orbital modulation of RX J0749 exhibits a

clear eclipse profile which seems to be closely resemble with R-band light curve. Though, both X-ray and optical observations are  $\sim 17$  years apart, their eclipse profiles provide a hint that both emissions are originating from the same region.

The double-humped periodic orbital modulations are also observed in the optical light curves of RX J0649 and are more prominent than that of the RX J0859. As described above these double humped variations suggest that both accreted poles of WD emit the radiations at various wavelengths. However, both humps are almost equally strong in all observations of RX J0649 which suggests that both poles accrete at the same rate. The photometric light curves of RX J0649 are very similar to the eclipsing polar WW Hor (Bailey et al. 1988) and EP Dra (Remillard et al. 1991) where the light curves show a well-defined eclipse profile as well as two symmetric prominent maxima. Similar to WW Hor and EP Dra, the presence of two maxima in RX J0649 could also be consistent with that produced by beaming of cyclotron emission towards the direction of the observer which further confirms the identification of this object as polar. At first sight the light curves of RX J0649 also show an eclipse that look similar to an eclipse of a WD. However, for the derived value of  $\Delta\phi_{ie}$  of  $0.15 \pm 0.03$ , the radius of the eclipsed source region is estimated to be  $\sim 55 R_{WD}$  with assumptions of  $i \sim 80^\circ$  and  $q = 0.54$  for an average value of the mass of WD of  $0.8 M_\odot$  for RXJ0649. Figure 12 also shows the variation of  $R$  as a function of  $q$  for RXJ0649. With an extreme high value of  $q$ ,  $R$  is estimated to be more than  $20 R_{WD}$ . This suggests that the hot accretion region is associated with the extended accretion stream and both are eclipsed by the secondary. The soft X-ray light curve of RXJ0649 was similar to its optical light curve, however, the eclipsed feature near the phase 0.0 in the X-ray light curve is shallower and narrow. Probably, this could be due to a smaller eclipsed region in the early epoch of observation.

The optical spectra of RX J0859, RX J0749, and RX J0649 are very similar to the spectra of other polars. They show strong emission lines of Balmer series, He I, and He II along with the conspicuous features of highly ionized optically thick regions like strong emission lines of He II 4686 Å and CIII/NIII. Presence of these emission lines in the optical spectra is a typical feature of AM Her systems (e.g. see Silber 1992). The magnetic nature of these systems can be further confirmed by the presence of an inverse Balmer decrement, a large value of EW of the  $H\beta$  ( $> 20$  Å), and the ratio of He II(4686)/ $H\beta > 0.4$  (see Silber 1992; Warner 1995). Both He II 4686 Å and  $H\beta$  emission lines during a significant fraction of the orbit (except during the eclipse) also demonstrates that the emission lines are formed in relatively compact regions which are illuminated by the strong photoionizing source like accretion column. The Balmer decrement,  $H\beta/H\alpha$  was estimated in the range of 1.1-1.3 for these three sources which suggests that the lower limit of electron density of the order of  $10^{12} \text{ cm}^{-3}$  (see Cropper 1990). These systems also appear to have been in relatively high states of accretion at the time of observations, as evidenced by the strength of their He II 4686 Å emission line (Patterson & Raymond 1985). Unlike Balmer emission lines, the Bowen fluorescence lines might be generated in these three sources due to the interaction of the X-rays with the surrounding gaseous matter in vicinity of the WD (see

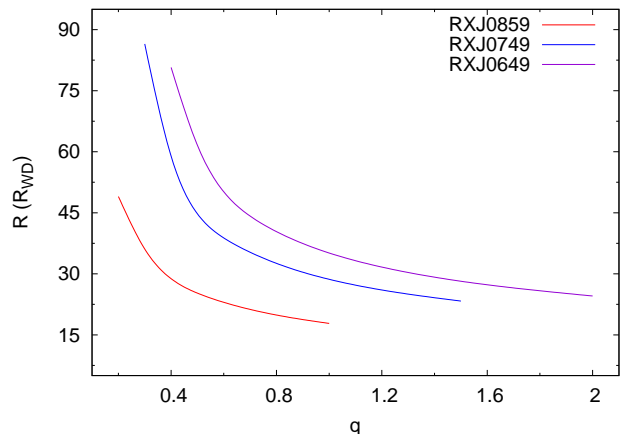


**Figure 12.** The plot of eclipsed size as a function of mass ratio for the polars RX J0859.1+0537, RX J0749.1-0549, and RX J0649.8-0737.

McClintock et al. 1975). The presence of the Bowen blend CIII/NIII together with the He II 4686 Å emission line in each spectrum also suggests that the regions where the lines originate possess a high-temperature (Schachter et al. 1991). The Fe II emission line is weak in the optical spectrum of RX J0749 and RX J0649, while almost absent in the spectrum of RX J0859. These Fe II emission lines could originate near the Roche lobe and be eclipsed by the secondary as the magnetic pole facing towards the observer. A similar behaviour has been observed in AM Herculis, where weak Fe II emission lines were also detected in the out-of-eclipse phase (see Schmidt et al. 1981).

Prominent broad emission humps are detected in the optical spectrum of each system. This could be due to the cyclotron emitting regions which are viewed almost perpendicularly near the limb of the white dwarf (Wickramasinghe et al. 1991). The identification of cyclotron humps in the optical spectra has revealed the magnetic field strength of about  $49 \pm 2$  MG,  $43.5 \pm 1.4$  MG, and  $44 \pm 1$  MG for RX J0859, RX J0749, and RX J0649, respectively, as is seen in many other polars. The cyclotron harmonics of RX J0859 and RX J0749 appear to closely resemble each other. In both systems, one cyclotron hump appears to be shallower than the other which could be observed due to the presence of the linear extension of the cyclotron emission region. The linearly extended cyclotron emission regions might be produced in the dispersed magnetic field, which could be responsible for the observed shallow feature in the optical spectrum of both RX J0859 and RX J0749 systems (Wickramasinghe et al. 1991).

## 5 CONCLUSIONS

We have determined the following properties of three poorly studied polars, namely RX J0859, RX J0749, and RX J0649, for the first time:

- All three X-ray sources are found to be eclipsing polars from their optical and X-ray observations.
- The orbital periods of RX J0859, RX J0749, and RX J0649 are  $2.393 \pm 0.003$  hrs,  $3.672 \pm 0.001$  hrs, and  $4.347 \pm 0.001$  hrs,

respectively. Among these systems, RX J0859 is found to lie in the region of the period gap, while RX J0749 and RX J0649 are found to lie above the period gap.

- The radius of the eclipsed light source is found to be more than the actual size of the WD in all the three polars, indicating that the eclipsed component is not only a WD but also an extended accretion stream or an extended magnetic region on the WD surface.
- The optical spectra of these systems are typical of polars, with strong high ionization emission lines and inverted Balmer decrement which confirms the magnetic nature of these systems.
- The observed cyclotron humps in the optical spectrum, lead to an estimate of the magnetic field strength of  $49\pm 2$  MG,  $43.5\pm 1.4$  MG, and  $44\pm 1$  MG for RX J0859, RX J0749, and RX J0649, respectively.

## 6 ACKNOWLEDGMENTS

We acknowledge the referee of this paper for his/her useful comments and suggestions. This research is based on the observations obtained by *ROSAT*, which has been supported by the Bundesministerium für Forschung und Technologie (BMFT) and the Max-Planck-Gesellschaft (MPG). One of the authors HPS thanks the Council of Scientific and Industrial Research (CSIR) for support.

## REFERENCES

- Bailey J., 1990, *MNRAS*, **243**, 57
- Bailey J., Cropper M., 1991, *MNRAS*, **253**, 27
- Bailey J., Wickramasinghe D. T., Hough J. H., Cropper M., 1988, *MNRAS*, **234**, 19P
- Barrett P. E., Chanmugam G., 1985, *ApJ*, **298**, 743
- Bernardini F., de Martino D., Mukai K., Falanga M., Masetti N., 2019, arXiv e-prints, p. [arXiv:1907.05318](https://arxiv.org/abs/1907.05318)
- Beuermann K., Burwitz V., Reinsch K., Schwöpe A. D., Thomas H.-C., 1995, in Bianchini A., della Valle M., Orío M., eds, *Astrophysics and Space Science Library* Vol. 205, *Cataclysmic Variables*. p. 381, [doi:10.1007/978-94-011-0335-0\\_112](https://doi.org/10.1007/978-94-011-0335-0_112)
- Beuermann K., Baraffe I., Kolb U., Weichhold M., 1998, *A&A*, **339**, 518
- Buckley D. A. H., Ferrario L., Wickramasinghe D. T., Bailey J. A., 1998, *MNRAS*, **295**, 899
- Cropper M., 1989, *MNRAS*, **236**, 935
- Cropper M., 1990, *Space Sci. Rev.*, **54**, 195
- Gaia Collaboration, Lindgren L., et al., 2018, *A&A*, **616**, A2
- Gänsicke B. T., Dillon M., 2009, *MNRAS*, **397**, 2170
- Hakala P. J., Watson M. G., Vilhu O., Hassall B. J. M., Kellett B. J., Mason K. O., Pirola V., 1993, *MNRAS*, **263**, 61
- Harrison T. E., Campbell R. K., 2015, *ApJS*, **219**, 32
- Horne J. H., Baliunas S. L., 1986, *ApJ*, **302**, 757
- Howell S. B., Craig N., Roberts B., McGee P., Sirk M., 1997, *AJ*, **113**, 2231
- Ingham W. H., Brecher K., Wasserman I., 1976, *ApJ*, **207**, 518
- Knigge C., 2006, *MNRAS*, **373**, 484
- Lamb D. Q., Masters A. R., 1979, *ApJ*, **234**, L117
- Littlefield C., Cook L. M., Bersier D., Davitt S., Kalamarides D., 2016, *The Astronomer's Telegram*, **9764**, 1
- Lomb N. R., 1976, *Ap&SS*, **39**, 447
- Mason P. A., Wells N. K., Motosoledi M., Szkody P., Gonzalez E., 2019, arXiv e-prints, p. [arXiv:1906.07767](https://arxiv.org/abs/1906.07767)
- McClintock J. E., Canizares C. R., Tarter C. B., 1975, *ApJ*, **198**, 641
- Motch C., et al., 1998, *A&AS*, **132**, 341
- Nauenberg M., 1972, *ApJ*, **175**, 417
- Pandel D., Cordova F. A., Shirey R. E., Ramsay G., Cropper M., Mason K. O., Much R., Kilkenny D., 2002, *MNRAS*, **332**, 116
- Patterson J., Raymond J. C., 1985, *ApJ*, **292**, 550
- Remillard R. A., Stroozas B. A., Tapia S., Silber A., 1991, *ApJ*, **379**, 715
- Ritter H., Kolb U., 2003, *A&A*, **404**, 301
- Roberts D. H., Lehar J., Dreher J. W., 1987, *AJ*, **93**, 968
- Sagar R., et al., 2011, *Current Science*, **101**, 1020
- Scargle J. D., 1982, *ApJ*, **263**, 835
- Schachter J., Filippenko A. V., Kahn S. M., Paerels F. B. S., 1991, *ApJ*, **373**, 633
- Schmidt G. D., Stockman H. S., Margon B., 1981, *ApJ*, **243**, L157
- Schwarz R., Greiner J., 1999, in Hellier C., Mukai K., eds, *Astronomical Society of the Pacific Conference Series* Vol. 157, *Annapolis Workshop on Magnetic Cataclysmic Variables*. p. 139 ([arXiv:astro-ph/9809399](https://arxiv.org/abs/astro-ph/9809399))
- Schwarz R., Greiner J., Tovmassian G. H., Zharikov S. V., Wenzel W., 2002, *A&A*, **392**, 505
- Schwöpe A. D., 1990, in Klare G., ed., *Reviews in Modern Astronomy* Vol. 3, *Reviews in Modern Astronomy*. pp 44–59, [doi:10.1007/978-3-642-76238-3\\_5](https://doi.org/10.1007/978-3-642-76238-3_5)
- Silber A. D., 1992, PhD thesis, MASSACHUSETTS INSTITUTE OF TECHNOLOGY.
- Silva K. M. G., Rodrigues C. V., Oliveira A. S., Almeida L. A., Cieslinski D., Costa J. E. R., Jablonski F. J., 2015, *MNRAS*, **451**, 4183
- Sinhal S. D., Kandpal C. D., Mahra H. S., Joshi S. C., Srivastava J. B., 1975, in Karandikar R. V., Alladin S. M., Sastry K. S., Abhyankar K. D., eds, *Optical Astronomy with Moderate Size Telescopes*. pp 20–34
- Smith D. A., Dhillon V. S., 1998, *MNRAS*, **301**, 767
- Staudte A., Schwöpe A. D., Schwarz R., 2001, *A&A*, **374**, 588
- Stobie R. S., Okeke P. N., Buckley D. A. H., O'Donoghue D., 1996, *MNRAS*, **283**, L127
- Szkody P., et al., 2005, *AJ*, **129**, 2386
- Vogel J., Schwöpe A. D., Gänsicke B. T., 2007, *A&A*, **464**, 647
- Warner B., 1995, *Cambridge Astrophysics Series*, **28**
- Watson M. G., et al., 1995, *MNRAS*, **273**, 681
- Wickramasinghe D. T., Meggitt S. M. A., 1982, *MNRAS*, **198**, 975
- Wickramasinghe D. T., Cropper M., Mason K. O., Garlick M., 1991, *MNRAS*, **250**, 692
- Woelk U., Beuermann K., 1992, *A&A*, **256**, 498
- Zombeck M. V., David L. P., Harnden F. R., Kearns K., 1995, in Siegmund O. H., Vallerger J. V., eds, *Proc. SPIE* Vol. 2518, *EUV, X-Ray, and Gamma-Ray Instrumentation for Astronomy VI*. pp 304–321, [doi:10.1117/12.218385](https://doi.org/10.1117/12.218385)
- Zorotovic M., Schreiber M. R., Gänsicke B. T., 2011, *A&A*, **536**, A42